Design and Fabrication of Novel Membranes for Advanced Water Desalination and Treatment

Sarah Tariq Alahmadi

Supervised by: Dr. Mohammed Obaid · Prof. Noreddine Ghaffour

King Abdullah University of Science and Technology (KAUST), Thuwal, Kingdom of Saudi Arabia

Abstract

Nanofiltration (NF) is widely used for dye separation; however, achieving high selectivity while maintaining water transport remains a major challenge. In this work, a bipyridine-based polyaminal network (Bipy-PAN), a nitrogen-rich porous organic polymer, was deposited onto a commercial PVDF ultrafiltration (UF) membrane as a selective layer using a simple vacuum-filtration approach. Bipy-PAN/UF membranes were prepared at different polymer loadings and characterized by X-ray diffraction (XRD), attenuated total reflectance Fourier-transform infrared spectroscopy (ATR-FTIR), and scanning electron microscopy (SEM). Cross-sectional SEM provided clear morphological evidence of Bipy-PAN deposition, while XRD confirmed the predominantly amorphous structure of Bipy-PAN and ATR-FTIR spectra of the modified membranes remained dominated by the UF support. Membrane performance was evaluated by dead-end filtration using Congo Red (CR), with the bare UF support and a commercial NF membrane used as references. Increasing Bipy-PAN loading enhanced CR rejection while reducing permeate flux, demonstrating a clear rejection–transport trade-off. The 10 mg membrane provided the best overall balance and achieved near-complete CR rejection. The optimized membrane was further tested with Methylene Blue (MB) and Acid Red 1 (AR1), which showed substantially lower rejection than CR. Despite their opposite charges, MB and AR1 exhibited relatively similar rejection, whereas the much larger CR was strongly retained, suggesting that molecular size played a more prominent role than dye charge under the investigated conditions. Overall, the results demonstrate that vacuum-assisted deposition of Bipy-PAN onto a commercial UF support can produce a selective polymer-modified membrane with nanofiltration-type dye-separation behavior, while highlighting the importance of optimizing polymer loading to balance dye rejection and water transport.

Contents

1 Introduction 4

2 Related Work 5

2.1 Porous Organic Polymers for Separation Applications 5

2.2 POP- and Porous-Material-Based Membranes 5

2.3 Nanofiltration Membrane Fabrication and Surface Modification 6

2.4 Nanofiltration Membranes for Dye Separation 6

2.5 Factors Governing Dye Rejection 7

2.6 Previous Work on Bipy-PAN 7

2.7 Research Positioning 8

3 Methodology 9

3.1 Materials and Membrane Fabrication 9

3.1.1 Materials 9

3.1.2 UF Substrate Pretreatment 9

3.1.3 Bipy-PAN Dispersion Preparation 9

3.1.4 Membrane Fabrication by Vacuum Filtration 10

3.1.5 Membrane Drying 10

3.1.6 Membrane Characterisation 10

3.2 Evaluation Procedure 10

3.2.1 Membrane Compaction 10

3.2.2 Dead-End Dye Filtration 10

3.2.3 Pure-Water Flux and Permeability Testing 10

3.2.4 UV–Vis Analysis 11

3.2.5 Performance Calculations 11

4 Results 11

4.1 Structural Characterisation 11

4.1.1 X-ray Diffraction 11

4.1.2 ATR-FTIR Spectroscopy 12

4.2 Morphological Characterisation 13

4.2.1 Bipy-PAN Morphology 13

4.2.2 UF Support Surface 13

4.2.3 Bipy-PAN-Modified Membrane Surface 14

4.2.4 Cross-Sectional Morphology 14

4.2.5 Membrane Appearance 15

4.3 Effect of Bipy-PAN Loading on Membrane Performance 16

4.4 UV–Vis Analysis 17

4.5 Dye Separation Performance 18

5 Discussion 19

5.1 Evidence of Bipy-PAN Deposition and Membrane Modification 19
5.2 Effect of Bipy-PAN Loading on Membrane Performance 20
5.3 Relationship Between Flux and Dye Rejection 21
5.4 Influence of Dye Molecular Properties and Membrane Dye Interactions 21
5.5 Comparison with UF Support and the Commercial NFX Reference 22
6 Limitations and Future Work 22
7 Conclusion 23
References 25

1 Introduction

Access to clean water is among the most pressing global challenges, and the fraction of the planet's water that is readily available as fresh water is very small relative to total global water resources, a situation that continues to be aggravated by rapid industrial expansion [4]. Membrane-based separation has become one of the principal responses to this problem, because it can separate dissolved species continuously, at moderate energy cost and with comparatively low chemical demand relative to conventional treatment trains [2].

Within the membrane family, nanofiltration (NF) occupies a distinctive position. NF membranes typically exhibit low retention of monovalent salts while retaining multivalent ions and organic molecules efficiently, a behaviour that arises from the combined action of steric size-sieving and Donnan electrostatic exclusion [1]. This combination makes NF particularly well suited to separations in which a comparatively small organic solute must be removed from a stream whose ionic content may be allowed to pass. Most commercial NF membranes are polyamide thin-film composites which generally carry a negative surface charge in commonly encountered feed solutions, and this charge state limits their effectiveness towards multivalent cations and cationic small molecules through charge neutralisation or electrostatic attraction [1].

A recurring obstacle in membrane development is the trade-off between permeability and selectivity: modifications that improve solute retention frequently reduce water transport. Adjusting surface charge, hydrophilicity and effective pore size is therefore central to lowering hydrodynamic resistance while improving purification performance [5]. Reported strategies include the incorporation of additives, surface coatings, chemical cross-linking and the construction of engineered interlayers [1]. Among the materials investigated for this purpose, porous organic polymers (POPs) and covalent organic frameworks (COFs) are attractive because of their tunable pore structures, high specific surface areas, and chemical and thermal stability [2], [6]. Selective layers built from such frameworks can provide uniform, hydrophilic and charge-modulated transport pathways which reduce mass-transfer resistance and bridge structural defects in the underlying support [7].

Dye-containing wastewater is one of the most widely studied applications of these engineered selective layers. Effluents from textile, printing and paper industries contain synthetic dyes that are toxic and, in many cases, carcinogenic, and their discharge poses a significant hazard to aquatic ecosystems and public health [6], [7]. Of the more than 700,000 tons of organic dyes produced globally each year, on the order of 200,000 tons are estimated to be discharged into the environment [7]. The efficiency with which a membrane rejects a given dye is governed by several interacting factors: the molecular size and weight of the dye relative to the effective pore size of the selective layer, the charge carried by both dye and membrane surface, adsorption of the solute onto the membrane, and the thickness and regularity of the selective layer itself [4], [5], [7]. Size exclusion acts as the primary barrier when the molecular dimensions of a dye exceed the effective nanochannel width, while Donnan exclusion causes charged membrane surfaces to repel like-charged solutes [1], [4]. Electrostatic adsorption of cationic dyes onto negatively charged surfaces adds a further complication, since it can simultaneously block water-intake channels and alter the local surface charge experienced by subsequent solutes [4], [5].

The present work examines whether a nitrogen-rich porous organic polymer can be used to convert a commercially available ultrafiltration support into a membrane with markedly improved dye retention,

using a fabrication route that is simple, reproducible and free of any in-situ chemical reaction. The polymer selected is Bipy-PAN, a bipyridine-based polyaminal network whose synthesis, structure and porosity have been reported previously by Alkayal et al. [3]. Bipy-PAN was deposited onto a commercial PVDF UF substrate by vacuum filtration, a physical deposition method, and the amount of polymer deposited was varied systematically. The resulting membranes were characterised structurally and morphologically, and their separation performance was evaluated in a dead-end filtration cell against Congo Red, with a UF support and a commercial polyamide NF membrane included as experimental references. The optimised membrane was subsequently evaluated against two further dyes of differing molecular weight and charge.

2 Related Work

2.1 Porous Organic Polymers for Separation Applications

Porous organic polymers constitute a broad class of highly cross-linked materials assembled from purely organic building blocks connected through strong covalent bonds [2]. The rigidity of this architecture, combined with the structural versatility of the available monomers, gives POPs permanent porosity, high specific surface areas, low density and good chemical and thermal stability across a range of solvents and pH values [2]. Unlike materials that collapse when guest molecules are removed, POPs retain their skeletal structure upon desolvation. According to their network configuration and synthetic route, POPs are commonly subdivided into covalent triazine frameworks, conjugated microporous polymers, hyper-cross-linked polymers and covalent organic frameworks [2].

Melamine-based networks have attracted particular attention within this family because of their inexpensive precursors, straightforward synthesis, high nitrogen content and adjustable basic functionality [2]. The electron-donating character of the triazine ring enhances the basicity of the attached primary amino groups, which allows melamine to interact with other functional groups through hydrogen bonding, metal coordination and π–π stacking [2]. Under suitable polymerisation conditions melamine reacts with aldehydes, carboxylic acids, acid dianhydrides and ketones to yield polyaminal, polyamide, polyimide and polyimine networks respectively [2]. Polyaminal networks in particular are typically obtained through a simple catalyst-free one-pot polycondensation of melamine with multi-aldehyde building blocks; this Schiff-base chemistry produces stable aminal linkages and hierarchical porous skeletons that have proved effective for gas capture, toxic-metal removal and heterogeneous catalysis [2].

2.2 POP- and Porous-Material-Based Membranes

To address the permeability–selectivity trade-off, porous organic polymers and related crystalline frameworks have been incorporated into membrane selective layers in several distinct ways [4], [6], [7]. Mixed-matrix membranes, in which porous nanoparticles such as zeolitic imidazolate frameworks, silicates, carbon nanotubes or COFs are blended into an organic polymer matrix, provide regular low-resistance nanochannels that enhance size-sieving and water transport [6]. Their principal weakness is dispersion: at high nanoparticle loadings, agglomeration generates non-selective voids and boundary gaps that degrade selectivity [6].

In-situ growth and interfacial assembly were developed partly to avoid these dispersion problems, allowing continuous crystalline selective layers to be constructed directly on ceramic or polymeric

supports [6]. COF-300 nanofiltration membranes grown in situ on ceramic tubular supports demonstrate precise molecular sieving, although the hydrophobic framework and narrow native pores of COF-300 limit water flux [6]. Defect engineering offers a route around this limitation: introducing a monoaldehyde terminator during non-stoichiometric polymerisation tailors missing-linker defects into the lattice, widening the internal pore structure and exposing hydrophilic unreacted amino groups, which raises water permeance without sacrificing selectivity [6].

A further strategy combines COFs with graphene oxide membranes. Graphene oxide interlayers provide fast two-dimensional transport pathways but swell and destabilise in aqueous environments; in-situ confined interfacial polymerisation of a COF within those interlayers simultaneously expands the interlayer spacing, strengthens inter-platelet interactions and increases surface hydrophilicity [7]. The in-plane pores of the intercalated COF act as short vertical transport pathways that shorten the tortuous diffusion path characteristic of graphene oxide membranes [7].

2.3 Nanofiltration Membrane Fabrication and Surface Modification

Nanofiltration membranes are prepared and modified by a range of established methods, including interfacial polymerisation, phase inversion, layer-by-layer deposition, chemical cross-linking, co-deposition and vacuum filtration [1]. Interfacial polymerisation dominates industrial manufacture, forming an ultrathin dense polyamide layer through reaction at a solvent interface between an aqueous monomer such as piperazine or polyethyleneimine and an organic monomer such as trimesoyl chloride [1]. Phase inversion is widely used to produce asymmetric microfiltration and ultrafiltration supports but remains difficult to apply to dense defect-free NF layers with high flux [1]. Layer-by-layer deposition exploits electrostatic interactions between alternating oppositely charged polyelectrolytes to build thin, charge-tunable selective layers [1], while chemical cross-linking forms a stable three-dimensional network that improves mechanical and chemical stability [1]. Co-deposition using polydopamine or phenolic amine chemistry allows rapid surface modification through spontaneous polymerisation under alkaline conditions [1].

Vacuum filtration is a well-established laboratory route to two-dimensional and composite membranes, in which suspended material is physically deposited onto an ultrafiltration or microfiltration support by liquid-phase suction [1], [4], [7]. Because the deposit is assembled by convective transport of the suspension towards the support, the method is simple, requires no chemical reaction and allows the deposited amount to be controlled directly through the concentration and volume of the filtered dispersion. Its principal limitation is that permeability depends strongly on the amount of material deposited: as the filtered volume increases, transport pathways lengthen and become more tortuous, increasing friction resistance and reducing permeation flux [4]. Surface charge and hydrophilicity modifications have been widely explored to offset this effect, since adjusting the surface zeta potential and enlarging water-intake entrances can improve both permeability and rejection without additional complex chemical treatment [5].

2.4 Nanofiltration Membranes for Dye Separation

Nanofiltration is well matched to dye wastewater treatment because it retains low-molecular-weight organic colorants while allowing water and monovalent salts to pass rapidly at low operating pressures [7]. Loose nanofiltration membranes, with molecular weight cut-offs in the range of roughly 500 to

2000 Da, are especially advantageous where inorganic salts should pass freely while organic dyes are retained [7].

Custom-engineered membranes are conventionally benchmarked against model dyes of differing charge and molecular weight. Congo Red is a large divalent anionic dye with a molecular weight of approximately 697 g mol^{-1} and a reported hydrated molecular radius of 8.76 Å [7]; owing to its size and charge it is strongly retained by negatively charged graphene oxide and COF membranes through the combined action of size exclusion and Donnan repulsion, with in-situ grown defective COF-300 membranes reported to reject up to 98.32 % and COF@GO membranes achieving near-complete rejection [6], [7]. Methylene Blue is a considerably smaller cationic dye of molecular weight 319.85 g mol^{-1} and reported molecular dimensions of 1.6 × 0.8 nm [5]. Because it is positively charged, it readily adsorbs onto negatively charged membrane surfaces, which can initially block water nanochannels and increase transport resistance while also producing a local charge inversion that repels subsequent cationic solutes [4], [5].

Acid Red 1 (AR1) was also investigated in the present work as an additional anionic dye with molecular characteristics intermediate between Methylene Blue and Congo Red. Its inclusion, together with Methylene Blue and Congo Red, enabled the separation behaviour of the Bipy-PAN-modified membrane to be evaluated using dyes with different molecular properties. The experimentally measured rejection of these dyes is discussed in Sections 4.5 and 5.4.

2.5 Factors Governing Dye Rejection

The separation performance of nanofiltration membranes towards dyes arises from a combination of physical and chemical effects rather than from any single mechanism.

- Steric hindrance. Size exclusion is the primary barrier when the molecular dimensions of the solute exceed the effective pore size or nanochannel width of the selective layer, and rejection therefore tends to correlate positively with the molecular weight and hydrated radius of the dye [4], [7]. Smaller dyes such as Methyl Orange pass through readily and exhibit low rejection [4], [6].
- Electrostatic (Donnan) interactions. Negatively charged membranes repel anionic dyes and thereby prevent them from approaching the water-intake entrances, while positively charged membranes repel cationic solutes [1], [4], [7].
- Adsorption and concentration polarisation. Cationic dyes adsorb onto negatively charged oxygen-containing surface groups, partially blocking transport channels and causing flux decline, while simultaneously inducing a local charge inversion that can enhance the rejection of subsequent cationic molecules [4], [5]. At sufficient solute concentrations, concentration polarisation produces a gel layer at the membrane surface that severely reduces permeance [7].
- Selective-layer structure. The thickness, hydrophilicity and regularity of the selective layer determine both transport resistance and the presence of non-selective bypass routes; thicker layers increase tortuosity and resistance, while uniform defect-free layers suppress bypass of dye molecules [4], [6], [7].

2.6 Previous Work on Bipy-PAN

The polymer used in the present work has been described previously in the literature. Alkayal et al. reported the synthesis and characterisation of a bipyridine-based polyaminal network, designated Bipy-PAN, prepared through a one-pot catalyst-free polycondensation carried out under an inert argon atmosphere [3]. In their procedure, melamine (0.5 g) and [2,2′-bipyridine]-5,5′-dicarbaldehyde (0.7 g) were combined in 30 mL of anhydrous dimethyl sulfoxide and heated at 175 °C for 72 h; after cooling, the white solid was isolated, washed successively with dimethylformamide, dichloromethane and acetone, and dried under vacuum at 60 °C for 3 h, affording an 85 % yield [3]. This synthesis was reported in the literature and was not carried out as part of the present membrane-fabrication project.

Alkayal et al. confirmed the formation of a cross-linked polyaminal network by FT-IR spectroscopy: a broad absorption band at 3300 cm^{-1} was assigned to the secondary amine of the aminal moiety, while the primary amine stretching bands of melamine at 3470 and 3420 cm^{-1} and the aldehyde stretching band of the dialdehyde precursor at 1610 cm^{-1} disappeared upon polymerisation [3]. The aminal linkage was further evidenced by a characteristic band at 1340 cm^{-1} assigned to the C–N group and by the absence of azomethine C=N stretching near 1600 cm^{-1}, and the triazine ring was confirmed by characteristic absorptions at 1510 and 1490 cm^{-1} [3]. Solid-state ^{13}C CP/MAS NMR spectroscopy showed triazine ring carbons at 165.9 and 156 ppm and aminal methylene carbons at 55.4 ppm [3].

Powder X-ray diffraction of Bipy-PAN exhibited only a single broad diffraction feature centred near $2\theta \approx 20°$, indicating an amorphous material and confirming that the crystalline starting materials had been fully consumed [3]. Field-emission scanning electron microscopy revealed agglomerated particles with cotton-like structures [3]. Thermogravimetric analysis indicated stability up to 355 °C, with network breakdown above that temperature and gradual burning above 410 °C [3]. Nitrogen sorption at 77 K gave a type IV isotherm with a small H4 hysteresis loop, a Brunauer–Emmett–Teller surface area of 160.7 $m^2\ g^{-1}$, a t-plot external surface area of 153.3 $m^2\ g^{-1}$ and a total pore volume of 0.31 $cm^3\ g^{-1}$ for pores smaller than 37 nm at $p/p° = 0.94$ [3]. The reported application of the material was as a solid adsorbent for carbon dioxide capture, taking up 1.02 and 0.71 mmol g^{-1} of CO_2 at 273 and 298 K respectively under 1 bar, a performance attributed to the abundance of polar nitrogen-rich groups on the pore surfaces [3].

2.7 Research Positioning

The literature summarised above establishes that porous organic polymers and related frameworks can be used to modify the surface charge, hydrophilicity and transport properties of nanofiltration membranes [4], [5], [6], [7]. Several gaps nevertheless remain. The modulation of charge through the depth of the selective layer, as distinct from superficial surface grafting, has rarely been investigated [1]. Fouling behaviour and cleaning strategies for modified membranes under realistic wastewater conditions are also under-studied, since most work relies on simplified laboratory feeds [1]. Finally, the fabrication of advanced POP- and COF-based membranes remains largely restricted to laboratory scales, and robust evaluations of long-term stability under practical operating conditions are lacking [1], [6].

Against this background, Bipy-PAN itself has to date been reported only as a gas-adsorption material [3]; to the best of the available literature it has not been evaluated as a membrane selective-layer material for liquid-phase dye separation. The present work therefore addresses a specific and narrow question: whether a nitrogen-rich polyaminal network, deposited by simple vacuum filtration onto a ultrafiltration

support, can produce a membrane with useful dye-separation performance, and how the amount of deposited polymer governs the balance between rejection and flux.

3 Methodology

3.1 Materials and Membrane Fabrication

3.1.1 Materials

Bipy-PAN was prepared according to the procedure reported in the Bipy-PAN study [3]. The support membrane was a commercial Synder flat-sheet ultrafiltration membrane, model A6, of poly(vinylidene fluoride) (PVDF), supplied by Sterlitech Corporation. A commercial nanofiltration reference membrane was also tested: a Synder flat-sheet NFX polyamide thin-film composite (PA-TFC) nanofiltration membrane, supplied by Sterlitech Corporation, part number YMNFX3001, in a 305 × 305 mm sheet format.

Three dyes were investigated: Congo Red (CR), Methylene Blue (MB) and Acid Red 1 (AR1). Deionised (DI) water was used throughout for dispersion preparation, substrate pretreatment, membrane compaction and dye feed preparation.

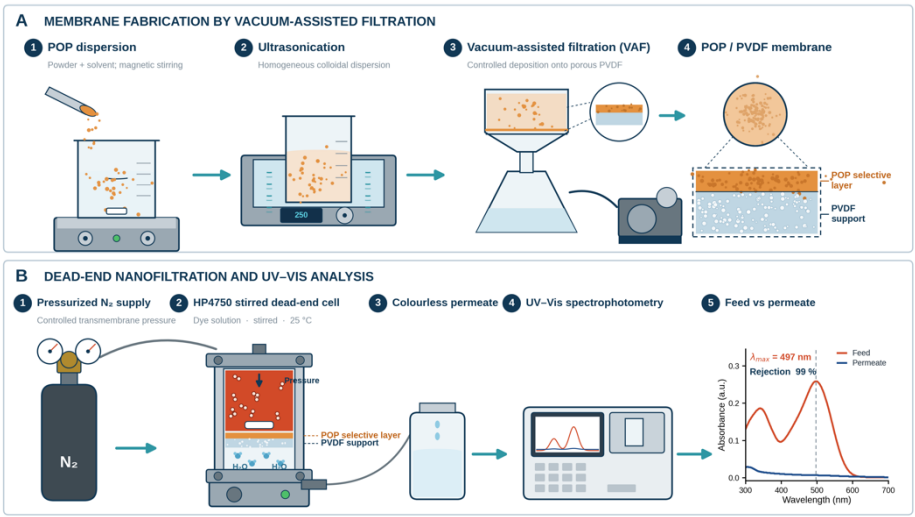


Figure 1. Schematic overview of Bipy-PAN/UF membrane fabrication and dye-filtration testing.

3.1.2 UF Substrate Pretreatment

The Synder A6 UF membrane was cut into circular coupons (1.8 cm diameter; effective area ≈ 2.54 cm²), rinsed and soaked in DI water, and kept wet until use. The pre-wetted UF substrates were subsequently mounted in the vacuum-filtration assembly for Bipy-PAN deposition.

3.1.3 Bipy-PAN Dispersion Preparation

Bipy-PAN dispersions were prepared at a fixed concentration of 0.5 mg mL^{-1} in DI water, corresponding to dispersion volumes of 5, 7, 10, 20 and 30 mL for polymer loadings of 2.5, 3.5, 5, 10 and 15 mg, respectively. Each dispersion was stirred for 5 min at 400 rpm and then sonicated for 30 min in a sonication bath; the bath power and frequency were not recorded. The dispersion was used for membrane fabrication by vacuum filtration immediately after sonication. The preparation sequence was therefore stirring, followed by bath sonication, followed by vacuum filtration.

3.1.4 Membrane Fabrication by Vacuum Filtration

The Bipy-PAN selective layer was deposited onto the pre-wetted Synder A6 UF support by vacuum filtration using a glass filtration assembly connected to a vacuum flask and vacuum pump. For each membrane, the entire volume of the prepared Bipy-PAN dispersion corresponding to the desired polymer loading was vacuum-filtered through a UF substrate. This process deposited Bipy-PAN onto the UF surface, forming a polymer-modified selective layer. Following deposition, the modified membranes were dried at room temperature for 12 h prior to characterization and filtration testing.

3.1.5 Membrane Drying

Following vacuum filtration, the fabricated polymer-modified membranes were dried for 12 h at room temperature.

3.1.6 Membrane Characterisation

The Bipy-PAN powder, bare UF support, and selected Bipy-PAN-modified membranes were characterized by X-ray diffraction (XRD), attenuated total reflectance Fourier-transform infrared spectroscopy (ATR-FTIR), and scanning electron microscopy (SEM). XRD was used to examine the structural characteristics of Bipy-PAN and to compare the diffraction patterns of the bare and modified membranes. ATR-FTIR spectroscopy was employed to examine the characteristic functional groups and spectral features of Bipy-PAN and the membrane samples. SEM was used to investigate the morphology of Bipy-PAN, UF support, and the polymer-modified membranes, including surface and cross-sectional morphology where available. The SEM acquisition conditions, including magnification, accelerating voltage, detector mode, and scale bar, are provided with the corresponding micrographs.

3.2 Evaluation Procedure

Membrane performance was evaluated using a stainless-steel dead-end filtration cell (Sterlitech Corporation) pressurized with argon gas. The experimental procedure included membrane compaction, dye-filtration testing, pure-water flux measurement, UV–Vis analysis, and calculation of dye rejection and permeate flux. Each experimental condition was evaluated in duplicate (n = 2), and the reported performance values represent the average of the two measurements.

3.2.1 Membrane Compaction

Prior to filtration testing, each membrane was compacted in the dead-end filtration cell using DI water at 4 bar for 1 min.

3.2.2 Dead-End Dye Filtration

Dye separation experiments were performed in the dead-end filtration cell at an operating pressure of 1 bar for 25 min. Circular membrane coupons with a diameter of 1.8 cm, corresponding to an effective filtration area of approximately 2.54 cm^2, were used with a feed volume of 150 mL and a dye concentration of 10 mg L^{-1}. Congo Red (CR) was initially used as the model dye to evaluate the effect of Bipy-PAN loading on membrane performance. Based on the resulting rejection–flux performance, the 10 mg Bipy-PAN/UF membrane was selected for subsequent evaluation using Congo Red, Methylene Blue (MB), and Acid Red 1 (AR1). The Synder A6 UF support and the commercial Synder NFX nanofiltration membrane were also evaluated as reference membranes.

3.2.3 Pure-Water Flux and Permeability Testing

A separate DI-water filtration test was performed independently of the compaction and dye-filtration experiments;

3.2.4 UV–Vis Analysis

The dye content of the feed and permeate solutions was assessed by ultraviolet–visible spectrophotometry using a UV-1900i UV–Vis spectrophotometer. Absorbance was measured at the wavelength selected experimentally for each dye: 499 nm for Congo Red, 666 nm for Methylene Blue, and 506 nm as the primary peak with 533 nm as a secondary peak for Acid Red 1.

3.2.5 Performance Calculations

Dye rejection was calculated directly from the measured feed and permeate absorbances without the use of a calibration curve. Under the Beer–Lambert law, absorbance is directly proportional to solute concentration in dilute solution at a fixed wavelength and path length; therefore, the ratio of permeate to feed absorbance was used in place of the corresponding concentration ratio [4]. Dye rejection was calculated according to Equation (1):

$$R\ (\%) = \left[1 - \frac{A_p}{A_f}\right] \times 100 \qquad (1)$$

where A_f and A_p are the UV–Vis absorbances of the feed and permeate solutions, respectively, measured at the selected wavelength.

The permeate collected during filtration was quantified gravimetrically by weighing. For the dilute aqueous dye solutions used in this study, a density of approximately 1.0 g mL^{-1} was assumed to convert the measured permeate mass to an equivalent permeate volume. Permeate flux was then calculated according to Equation (2):

$$J = V / (A \times t) \qquad (2)$$

where J is the permeate flux, V is the permeate volume, A is the effective membrane area (approximately 2.54 cm^2, equivalent to 2.54 x 10^{-4} m^2), and t is the filtration time (25 min, equivalent to 0.4167 h). Flux values are reported in L m^{-2} h^{-1} (LMH).

4 Results

4.1 Structural Characterisation

4.1.1 X-ray Diffraction

Figure 2 presents the XRD patterns of the Bipy-PAN powder, the bare UF support, and the Bipy-PAN-modified membranes prepared at 3.5, 5, 10 and 15 mg loadings. The Bipy-PAN powder shows no sharp reflections and instead exhibits a broad, low-intensity diffraction feature centred at approximately 2θ = 20–22°, consistent with the broad diffraction feature previously reported for Bipy-PAN [3].

The UF support displays three comparatively well-defined diffraction maxima located at approximately 2θ = 17.5°, 21° and 25.5°, together with a weaker feature near 2θ = 41°. The same main diffraction features occur at approximately the same angular positions in the Bipy-PAN-modified membranes. No

additional distinct diffraction maximum is resolved in the modified-membrane patterns, and no clear shift in the angular positions of the main UF reflections is observed.

The patterns differ in absolute intensity. The 3.5 and 10 mg patterns are close in intensity to that of the bare support, whereas the 5 and 15 mg patterns show markedly lower absolute intensities. The intensity differences are not monotonic with polymer loading. As the patterns were obtained from separately mounted membrane coupons and were neither offset nor normalised, differences in absolute intensity were not used to quantify polymer deposition.

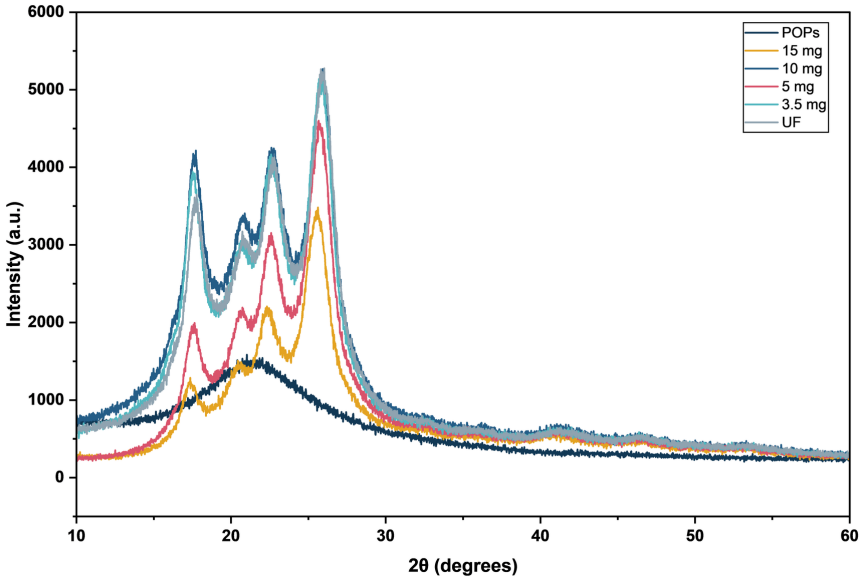


Figure 2. X-ray diffraction patterns of the Bipy-PAN powder (POPs), UF support, and Bipy-PAN/UF membranes prepared at 3.5, 5, 10 and 15 mg polymer loading.

4.1.2 ATR-FTIR Spectroscopy

Figure 3 shows the ATR–FTIR spectra of the Bipy-PAN powder, the bare UF support, and the Bipy-PAN-modified membranes prepared at 5, 10 and 15 mg loadings. The spectrum of the Bipy-PAN powder is distinct from the membrane spectra, exhibiting a broad absorption band centred near 3300–3400 cm^{-1}, a comparatively flat region between approximately 3000 and 1800 cm^{-1}, and multiple overlapping absorption bands in the fingerprint region. The broad band near 3300–3400 cm^{-1} is consistent with the secondary amine functionality of the aminal moiety reported for Bipy-PAN, while the absorption features in the fingerprint region are consistent with the triazine and C–N functionalities described in the literature [3].

In contrast, the spectra of the UF support and the Bipy-PAN-modified membranes are closely similar, with comparable prominent absorption features throughout the fingerprint region. No distinct additional band that can be confidently assigned to Bipy-PAN and distinguished from the underlying UF spectrum is clearly resolved in the modified membranes. Furthermore, no systematic spectral change with increasing polymer loading is apparent among the 5, 10 and 15 mg membranes.

Therefore, under the ATR–FTIR measurement conditions used in this work, the spectra of the modified membranes remain dominated by features associated with the underlying UF support. ATR–FTIR alone does not provide clear evidence of Bipy-PAN deposition, and evidence of membrane modification is considered together with the morphological observations obtained by SEM.

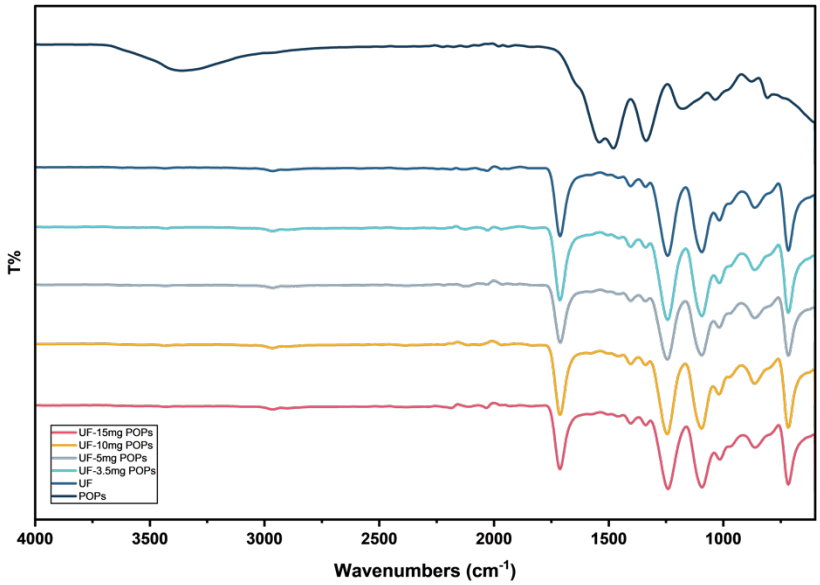


Figure 3. FTIR spectra of the Bipy-PAN powder (POPs), UF support, and Bipy-PAN/UF membranes prepared at 3.5, 5, 10 and 15 mg polymer loading.

4.2 Morphological Characterisation

4.2.1 Bipy-PAN Morphology

Figure 4 shows the SEM morphology of the Bipy-PAN powder at 71,000× magnification. The polymer exhibits an irregular, highly agglomerated particulate morphology, consisting of fine particles assembled into larger clusters. The surface appears rough and heterogeneous, with no well-defined regular particle geometry. This morphology is broadly consistent with the agglomerated, cotton-like morphology previously reported for Bipy-PAN by Alkayal et al. [3].

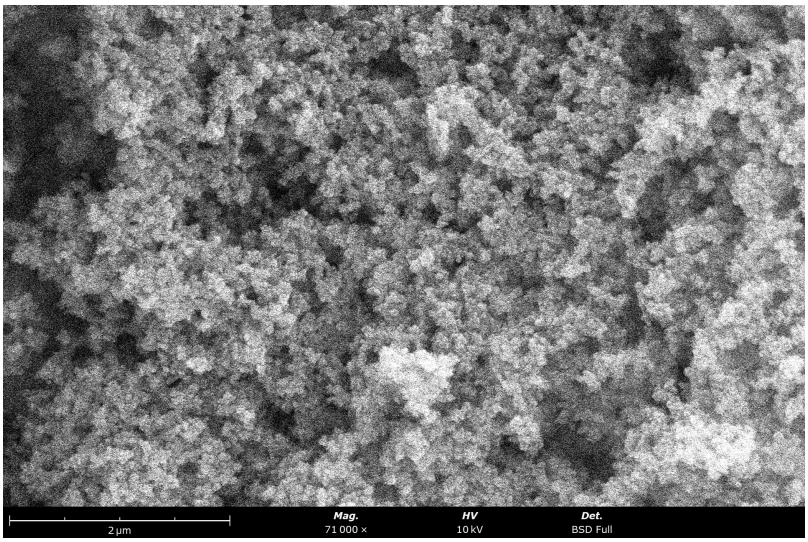


Figure 4. Scanning electron micrograph of the Bipy-PAN powder (71,000×, 10 kV, BSD detector, 2 µm scale bar).

4.2.2 UF Support Surface

Figure 5 shows the surface morphology of the bare Synder A6 UF support at 25,000× magnification. The membrane surface exhibits a relatively continuous matrix containing numerous dark, irregularly shaped openings distributed across the imaged area. These openings vary in size and appear randomly

distributed over the surface. This micrograph provides the morphological reference for comparison with the Bipy-PAN-modified membrane.

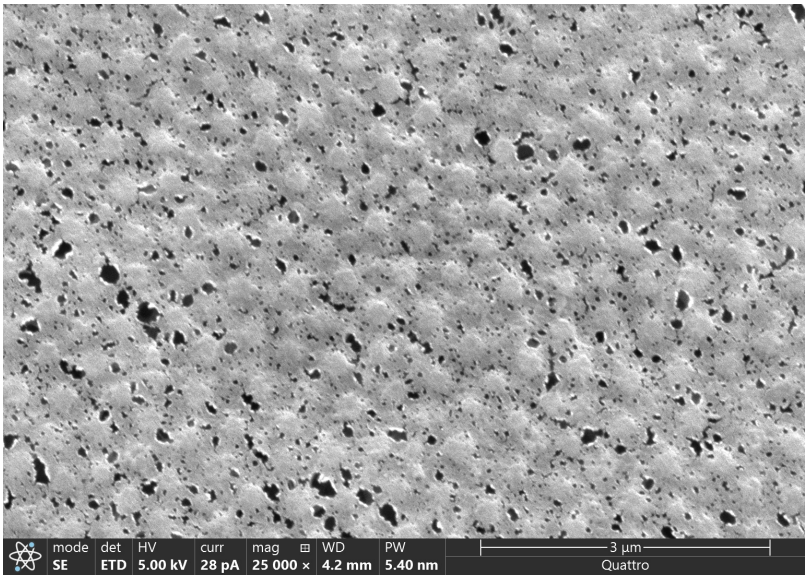


Figure 5. Scanning electron micrograph of the UF support surface (25,000×, 5.00 kV, ETD detector in secondary-electron mode, 3 µm scale bar).

4.2.3 Bipy-PAN-Modified Membrane Surface

Figure 6 shows the surface morphology of the Bipy-PAN/UF membrane prepared at a polymer loading of 2.5 mg and imaged at 1,550× magnification. The surface exhibits extensive aggregated particulate material distributed across the imaged area, with aggregates of different sizes forming a heterogeneous and irregular morphology. Several narrow, dark fissure-like features are also visible across the deposited material. Overall, the observed surface morphology is consistent with the presence of deposited Bipy-PAN on the UF support.

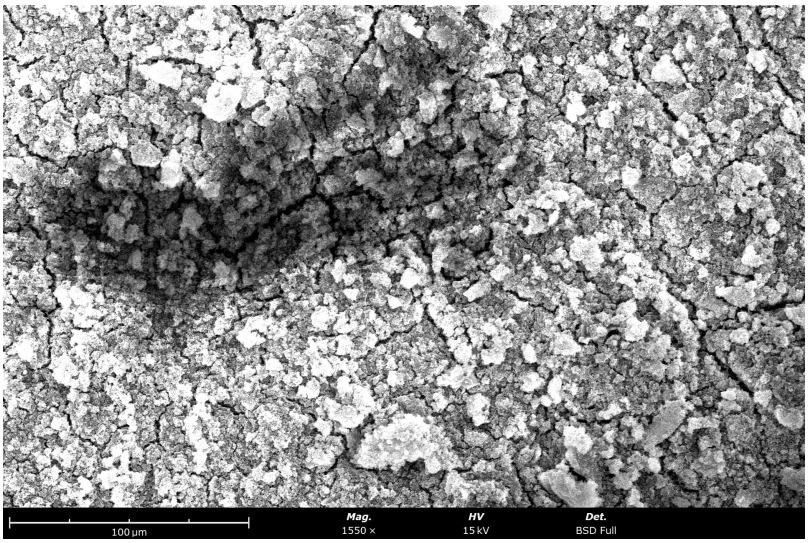


Figure 6. Scanning electron micrograph of the surface of the Bipy-PAN/UF membrane prepared at 2.5 mg loading (1,550×, 15 kV, BSD detector, 100 µm scale bar).

4.2.4 Cross-Sectional Morphology

Figure 7 presents cross-sectional SEM micrographs of the UF support and the Bipy-PAN/UF membranes prepared at polymer loadings of 3.5, 5, 10 and 15 mg. The bare UF support (panel a) shows a relatively uniform fractured cross-section without a distinct particulate outer region.

In contrast, the Bipy-PAN/UF membranes exhibit a granular, particulate-textured region along the outer side of the cross-section, which is distinguishable from the underlying UF support. This region is observed in all four modified membranes. At 3.5 mg (panel b), a rough outer region is visible along the membrane cross-section. At 5 mg (panel c), the particulate region becomes clearly distinguishable from the underlying support. The 10 mg membrane (panel d) shows a well-defined and continuous particulate outer region, while the 15 mg membrane (panel e) also exhibits a pronounced granular region along the membrane edge.

The presence of this outer particulate region in the Bipy-PAN/UF membranes, together with its absence from the bare UF support, provides clear morphological evidence of Bipy-PAN deposition on the UF substrate.

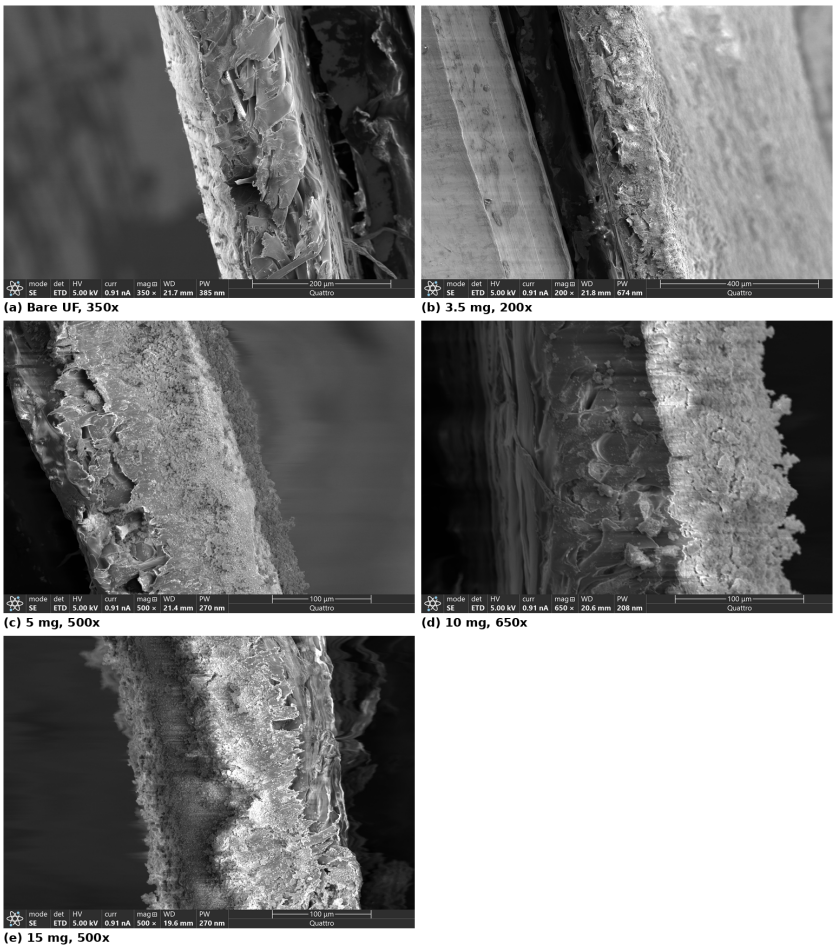


Figure 7. Cross-sectional scanning electron micrographs: (a) UF support, 350×; (b) Bipy-PAN/UF, 3.5 mg, 200×; (c) 5 mg, 500×; (d) 10 mg, 650×; (e) 15 mg, 500×. All images acquired at 5.00 kV using the ETD detector in secondary-electron mode. Scale bars are given individually in each panel.

4.2.5 Membrane Appearance

Figure 8 shows photographs of the Bipy-PAN/UF membranes prepared at 2.5, 5, 10 and 15 mg polymer loadings before and after Congo Red filtration. Before filtration, the membranes show a pale cream to light-yellow appearance across the deposition area. After filtration, a distinct coloured circular region corresponding to the active filtration area is visible on all membranes, indicating retention of Congo Red at the membrane surface. The intensity of the retained dye differs among the membranes, with the 5 mg membrane showing the most intense red coloration, while the 2.5, 10 and 15 mg membranes show lighter orange-to-red coloration. These visual differences are consistent with differences in dye retention among the tested polymer loadings.

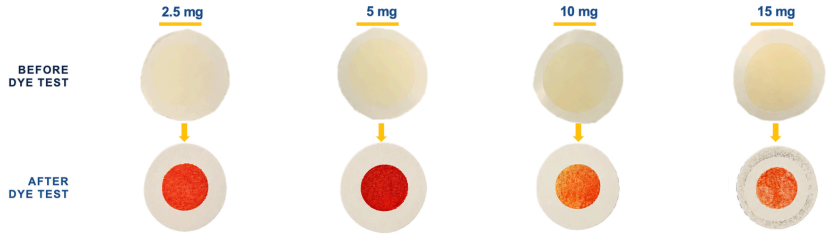


Figure 8. Photographs of the Bipy-PAN/UF membranes at 2.5, 5, 10 and 15 mg polymer loading, before and after the Congo Red dead-end filtration test.

Figure 9 shows the Congo Red feed solution and the permeate collected after dead-end filtration. The feed exhibits the characteristic orange-red colour of Congo Red, whereas the collected permeate appears visually clear. These photographs provide a qualitative visual comparison between the feed and permeate; quantitative dye rejection was determined separately using UV–Vis spectroscopy.

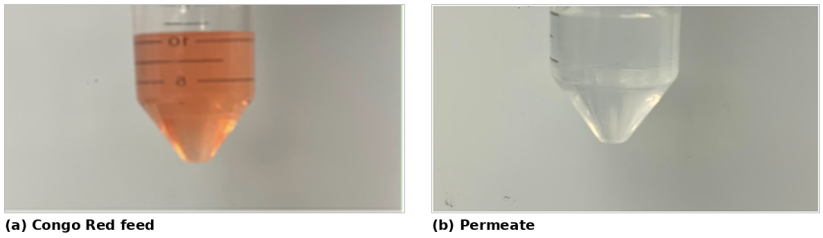


Figure 9. Visual comparison of the Congo Red feed solution (10 mg L^{-1}) and the corresponding permeate obtained after membrane filtration: (a) feed; (b) permeate.

4.3 Effect of Bipy-PAN Loading on Membrane Performance

Figure 10 presents the Congo Red rejection and permeate flux of the UF support, the commercial NFX nanofiltration reference, and the Bipy-PAN/UF membranes prepared at 2.5, 3.5, 5, 10 and 15 mg polymer loadings. All membranes were evaluated under the same dead-end filtration conditions using a 10 mg L^{-1} Congo Red feed at 1 bar for 25 min.

Congo Red rejection increased with increasing Bipy-PAN loading. The 2.5 mg membrane showed only a moderate improvement in rejection compared with the bare UF support, whereas a pronounced increase was observed at 5 mg. Rejection increased further at 10 mg, reaching nearly complete Congo Red retention, and only a small additional change was observed at 15 mg.

In contrast, permeate flux generally decreased as the Bipy-PAN loading increased. A substantial reduction in flux was observed after deposition of the polymer compared with the bare UF support. The flux decreased further from 2.5 to 5 mg, remained similar between 5 and 10 mg, and reached its lowest value at 15 mg. The commercial NFX membrane showed the highest measured flux among the tested membranes under the experimental conditions used in this study.

Considering rejection and permeate flux together, the 10 mg Bipy-PAN loading provided the most favourable performance balance. It achieved Congo Red rejection close to that obtained at 15 mg while maintaining substantially higher permeate flux. Therefore, the 10 mg Bipy-PAN/UF membrane was selected for the subsequent dye-separation experiments.

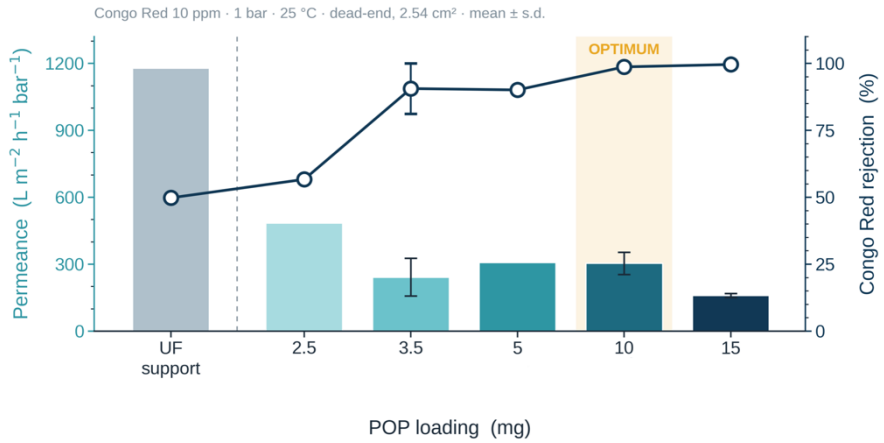


Figure 10. Congo Red rejection (left axis) and permeate flux (right axis) for the UF support, and the Bipy-PAN/UF membranes at 2.5, 3.5, 5, 10 and 15 mg polymer loading. Conditions: dead-end filtration, 1 bar, 25 min, 150 mL feed at 10 mg L^{-1} Congo Red, effective membrane area ≈ 2.54 cm^2.

4.4 UV–Vis Analysis

Figure 11 presents the UV–Vis absorbance spectra of the Congo Red feed solution and the permeates collected from the bare UF support, the commercial NFX reference membrane, and the Bipy-PAN/UF membranes prepared at 2.5, 5, 10 and 15 mg polymer loadings. The feed spectrum exhibits two main absorption bands, with the major absorption maximum occurring at approximately 500 nm. Congo Red rejection was evaluated at the experimentally selected wavelength of 499 nm.

All permeate samples show lower absorbance than the feed solution, indicating a reduction in Congo Red concentration after filtration. The UF, NFX and 2.5 mg permeates retain clearly visible absorption bands, whereas a substantial decrease in absorbance is observed for the 5 mg membrane. The absorbance is reduced further for the 10 and 15 mg membranes, with their spectra approaching the baseline near the characteristic Congo Red absorption maximum.

Overall, the progressive reduction in permeate absorbance with increasing Bipy-PAN loading is consistent with the increase in Congo Red rejection observed in Figure 10. In particular, the very low absorbance of the 10 and 15 mg permeates corresponds to their high Congo Red rejection. The positions of the main absorption bands remain approximately unchanged after filtration, while their intensities decrease substantially.

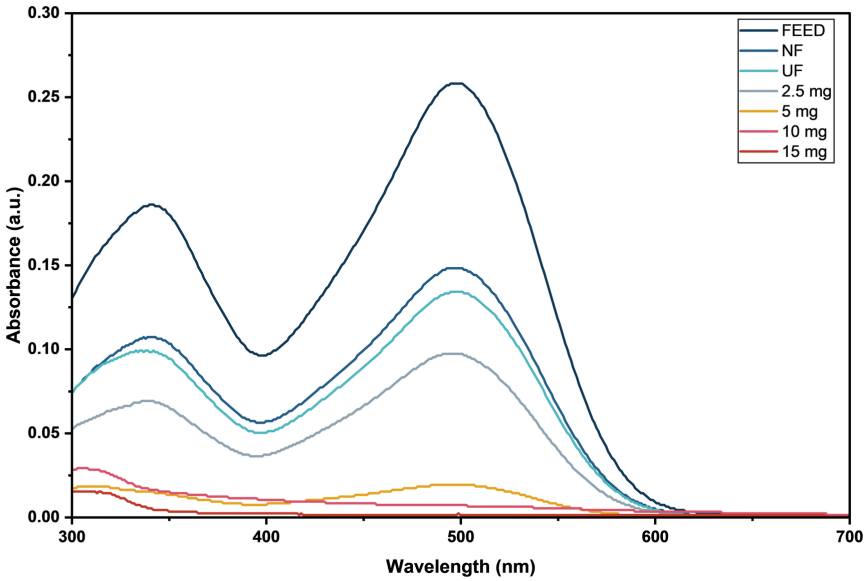


Figure 11. UV–Vis absorbance spectra of the Congo Red feed solution (10 mg L^{-1}) and of the permeates collected from the commercial NFX reference, UF support, and the Bipy-PAN/UF membranes at 2.5, 5, 10 and 15 mg loading.

4.5 Dye Separation Performance

Figure 12 compares the rejection of Methylene Blue (MB), Acid Red 1 (AR1), and Congo Red (CR) using the optimised 10 mg Bipy-PAN/UF membrane. All three dyes were evaluated under the same dead-end filtration conditions using a feed concentration of 10 mg L^{-1}.

A clear difference in rejection was observed among the three dyes. Congo Red showed the highest rejection, reaching nearly 100%, whereas Acid Red 1 and Methylene Blue exhibited considerably lower rejection values of approximately 25% and 20%, respectively. Thus, the optimised Bipy-PAN/UF membrane showed substantially greater retention of Congo Red than of the other two dyes.

When the rejection values are compared with the molecular weights of the dyes, the highest rejection corresponds to Congo Red, which has the largest molecular weight among the three dyes tested. Acid Red 1, with an intermediate molecular weight, and Methylene Blue, with the lowest molecular weight, showed much lower rejection. These results indicate that dye molecular size may play an important role in the observed separation behaviour of the Bipy-PAN/UF membrane.

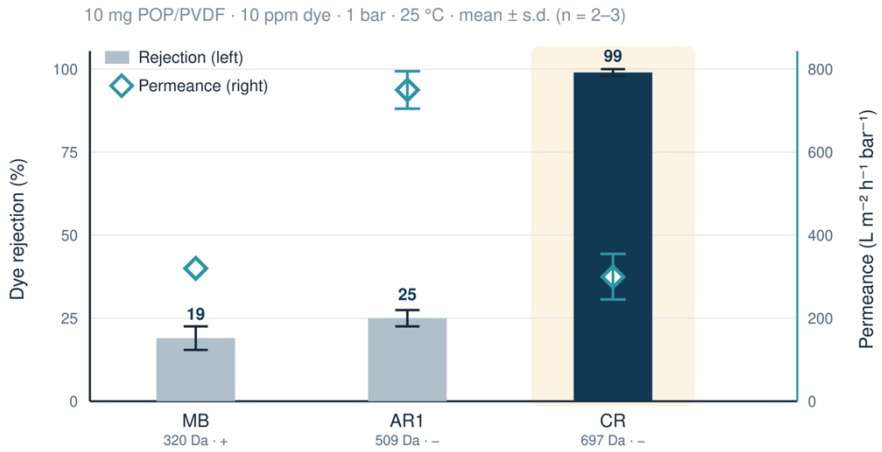


Figure 12. Rejection of Methylene Blue (MB), Acid Red 1 (AR1) and Congo Red (CR) by the optimised 10 mg Bipy-PAN/UF membrane, plotted against dye molecular weight. Conditions: dead-end filtration, 1 bar, 25 min, 150 mL feed at 10 mg L^{-1}, n = 2. Absorbance measured at 666 nm (MB), 506 nm (AR1) and 499 nm (CR).

The molecular properties of the three dyes, as far as these are supported by the literature consulted, are summarised in Table 1.

Dye	Molecular weight (g mol^{-1})	Charge state	Reported dimensions	Experimental λ used (nm)
Congo Red (CR)	≈ 697 [7]	Divalent anionic [7]	Hydrated radius 8.76 Å [7]	499
Methylene Blue (MB)	319.85 [5]	Cationic [5]	1.6 × 0.8 nm [5]	666
Acid Red 1 (AR1)	≈ 509.42 [8]	Anionic (disulfonated)[8]		506 (primary); 533 (secondary)

Table 1. Molecular properties of the dyes investigated.

5 Discussion

5.1 Evidence of Bipy-PAN Deposition and Membrane Modification

The characterization results provide complementary evidence for the modification of the UF support with Bipy-PAN. Among the techniques used, cross-sectional SEM provides the clearest morphological evidence of the deposited region, while ATR-FTIR and XRD provide additional structural information.

The cross-sectional SEM micrographs in Figure 7 show a clear difference between the bare UF support and the Bipy-PAN-modified membranes. The bare support exhibits a relatively uniform fractured structure, whereas the modified membranes show a distinct granular, particulate-textured region along one face of the substrate. This region is observed in the modified membranes prepared at 3.5, 5, 10 and 15 mg loadings and is absent from the bare UF support. The surface micrograph of the 2.5 mg membrane in Figure 6 also shows extensive coverage of the support by aggregated particulate material. Together, these observations are consistent with the deposition of Bipy-PAN onto the UF support during vacuum filtration.

The ATR-FTIR results provide less distinct evidence of membrane modification. Although the Bipy-PAN powder exhibits characteristic absorption features, the spectra of the modified membranes remain largely dominated by the bands of the underlying UF substrate. No additional band that can be clearly

assigned to Bipy-PAN is resolved in the modified-membrane spectra, and no systematic spectral change is observed with increasing polymer loading. Therefore, ATR-FTIR alone does not provide clear independent confirmation of Bipy-PAN deposition in the modified membranes.

The XRD results are consistent with the amorphous nature of Bipy-PAN reported in the literature [3]. The Bipy-PAN powder exhibits a broad diffraction feature around $2\theta \approx 20°$, while no additional distinct polymer-related diffraction maxima are resolved in the modified membranes. This is consistent with deposition of an amorphous material, although the XRD patterns alone cannot independently confirm its presence. Differences in absolute diffraction intensity among the modified membranes are non-monotonic with polymer loading and were therefore not interpreted as a quantitative indication of the amount of deposited polymer.

Overall, the characterization results indicate successful modification of the UF support. The SEM observations provide the strongest direct morphological evidence of the deposited Bipy-PAN region, while the ATR-FTIR and XRD results are consistent with the characteristics of the polymer and substrate but do not independently demonstrate deposition.

5.2 Effect of Bipy-PAN Loading on Membrane Performance

The results in Figure 10 demonstrate that Bipy-PAN loading has a pronounced effect on both Congo Red rejection and permeate flux. Increasing the polymer loading generally improves dye rejection while reducing permeate flux, indicating a clear trade-off between selectivity and water transport.

At the lowest tested loading of 2.5 mg, Congo Red rejection is only moderately higher than that of the bare UF support, while the permeate flux is substantially reduced. This suggests that the deposited amount at this loading modifies the transport characteristics of the UF support but does not yet provide the high dye retention observed at the higher loadings.

Increasing the Bipy-PAN loading from 2.5 to 5 mg produces a substantial increase in Congo Red rejection, accompanied by a further decrease in permeate flux. A further increase to 10 mg raises the rejection to near-complete levels, while the flux remains similar to that measured for the 5 mg membrane. These results indicate that increasing the amount of deposited Bipy-PAN progressively enhances the selective barrier to Congo Red transport. This general behaviour is consistent with previous reports in which increasing the amount of selective material improved solute rejection while increasing resistance to permeate transport [5,6].

Increasing the loading further from 10 to 15 mg produces only a small change in Congo Red rejection, which remains close to complete, whereas the permeate flux decreases substantially. Therefore, the additional polymer deposited at 15 mg provides little further improvement in dye rejection while imposing a considerably greater resistance to permeate transport.

Considering rejection and permeate flux together, the 10 mg membrane provides the most favourable performance among the loadings tested. It achieves Congo Red rejection close to that of the 15 mg membrane while retaining approximately twice its permeate flux. The selection of 10 mg as the optimum loading is therefore based on the combined rejection–flux performance rather than on rejection alone.

Overall, the results show that increasing Bipy-PAN loading improves Congo Red rejection up to approximately 10 mg, beyond which the rejection approaches a plateau while permeate flux continues to decrease.

5.3 Relationship Between Flux and Dye Rejection

Across the Bipy-PAN loading series, permeate flux and Congo Red rejection generally changed in opposite directions. Increasing the polymer loading resulted in higher dye rejection, while the permeate flux progressively decreased. This behaviour reflects the commonly reported permeability–selectivity trade-off in membrane separation, where improved solute retention is often accompanied by reduced permeate transport [1], [5], [7].

The relationship between flux and rejection was not proportional across the loading series. Between 5 and 10 mg, Congo Red rejection increased substantially while the permeate flux changed only slightly. In contrast, increasing the loading from 10 to 15 mg produced little additional improvement in rejection but caused a pronounced decrease in flux. Therefore, the highest polymer loading did not provide the most favourable overall membrane performance.

Considering both separation and transport performance, the 10 mg Bipy-PAN/UF membrane provided the best balance among the tested loadings. At this loading, Congo Red rejection was close to that obtained with the 15 mg membrane, while the permeate flux remained approximately twice as high. These results demonstrate that membrane performance should be evaluated using both rejection and flux rather than rejection alone.

5.4 Influence of Dye Molecular Properties and Membrane Dye Interactions

The three-dye comparison in Figure 12 shows a clear increase in rejection with molecular weight, with the most pronounced difference occurring between Acid Red 1 and Congo Red. Congo Red is the largest of the three dyes by molecular weight and has a reported hydrated molecular radius of 8.76 Å [7]. Its near-complete rejection by the optimised membrane is consistent with an important contribution from molecular size and size-exclusion effects, which have also been reported in the separation of Congo Red by graphene oxide- and COF-based membranes [6], [7].

The behaviour of the two smaller dyes provides additional insight into the possible influence of charge. Methylene Blue is cationic, whereas Acid Red 1 is an anionic dye [8], yet both showed relatively low and similar rejection compared with Congo Red. If electrostatic interactions were the dominant factor controlling separation, a stronger difference between oppositely charged dyes might be expected, as Donnan exclusion can influence the transport of charged solutes through charged membrane surfaces [1], [4]. The observed rejection trend therefore suggests that molecular size may have played a more prominent role than dye charge under the conditions investigated. However, this interpretation remains tentative because the surface charge of the Bipy-PAN/UF membrane was not measured and the feed pH was neither measured nor adjusted. Consequently, the contribution of electrostatic interactions cannot be quantified from the present data.

Adsorption may also contribute to the observed separation behaviour. Interactions between dye molecules and membrane surfaces can influence apparent dye retention and permeate transport [4], [5]. However, adsorption was not measured independently in the present work, and therefore its contribution cannot be distinguished from membrane rejection based on the available filtration data.

Acid Red 1 (AR1) was experimentally evaluated as the intermediate-molecular-weight dye in this study. The literature reports a molecular formula of $C_{18}H_{13}N_3Na_2O_8S_2$, a molecular weight of 509.42 g mol^{-1}, and a maximum absorption wavelength of approximately 532 nm [8]. These reported properties support its identification and molecular-weight placement in the three-dye comparison. Its rejection under the present membrane-filtration conditions, however, is derived solely from the experimental results of this work.

5.5 Comparison with UF Support and the Commercial NFX Reference

Relative to the UF support, all Bipy-PAN-modified membranes showed improved Congo Red rejection, with the improvement becoming particularly pronounced at polymer loadings of 5 mg and above. The 10 and 15 mg membranes achieved near-complete Congo Red rejection, demonstrating the substantial improvement in dye retention obtained after deposition of the Bipy-PAN layer. This improvement was accompanied by a reduction in permeate flux, consistent with the rejection–flux behaviour discussed in Sections 5.2 and 5.3.

The commercial Synder NFX nanofiltration membrane was evaluated under the same experimental conditions as an additional reference. Under the conditions used in this study, the NFX membrane exhibited a high measured permeate flux and Congo Red rejection comparable to that of the UF support. The UV–Vis spectra in Figure 11 are consistent with the measured rejection results, with the NFX and UF permeates showing substantially higher absorbance than those obtained from the higher-loading Bipy-PAN/UF membranes.

Overall, comparison with the UF support demonstrates the effect of Bipy-PAN deposition most clearly. The substantial increase in Congo Red rejection, particularly at the 10 mg loading, shows that vacuum-assisted deposition of Bipy-PAN can provide the UF support with enhanced dye-separation performance while retaining measurable permeate flux.

6 Limitations and Future Work

Several limitations of the present study should be considered when interpreting the results and provide directions for future work.

* Feed pH and membrane surface charge were not measured. Because electrostatic interactions between dyes and membrane surfaces depend on solution conditions and surface charge, the contribution of charge-based separation could not be determined quantitatively. Future work should include controlled-pH filtration experiments together with zeta-potential measurements to distinguish the relative contributions of molecular size and electrostatic interactions.

* Selective-layer thickness and surface wettability were not quantified. Although cross-sectional SEM showed a distinguishable deposited region on the modified membranes, quantitative layer-thickness measurements were not performed. Future studies could combine calibrated cross-sectional imaging with contact-angle measurements to relate membrane structure and surface properties to separation performance.

* The morphological characterisation was not identical for all polymer loadings. Cross-sectional SEM was available for the 3.5, 5, 10 and 15 mg membranes, whereas surface SEM was obtained only for the

2.5 mg modified membrane and the bare UF support. A systematic surface and cross-sectional SEM series acquired under comparable imaging conditions would provide a more complete assessment of morphological changes with polymer loading.

* The three-dye comparison was performed only using the optimised 10 mg membrane. Therefore, the effect of polymer loading on the separation of Methylene Blue and Acid Red 1 was not investigated. Testing all three dyes across multiple polymer loadings would provide a more comprehensive understanding of the relationship between membrane loading and dye properties.

* Each filtration condition was evaluated in duplicate (n = 2), and standard deviations were not calculated. Additional independent replicates and statistical analysis would improve the assessment of experimental variability and strengthen comparisons between neighbouring polymer loadings.

* The commercial NFX membrane showed an unusual experimental response under the conditions used in this study. Repeating the NFX experiment with additional membrane coupons would help determine the reproducibility of the measured performance and provide a more robust commercial NF comparison.

* The filtration experiments were conducted at a single dye concentration and operating pressure over relatively short filtration periods. Future work should examine a wider range of feed concentrations and pressures, together with longer-term and multi-cycle filtration tests, to evaluate membrane stability, flux recovery and performance under extended operation.

* Salt separation was not evaluated in the present experiments. Since the modified membrane is intended to provide nanofiltration-type separation performance, future work should include rejection measurements using representative salts to assess its performance beyond dye separation.

7 Conclusion

This work investigated the use of a bipyridine-based polyaminal network (Bipy-PAN) as a selective layer deposited onto a commercial ultrafiltration (UF) support for enhanced dye separation. Bipy-PAN-modified membranes were fabricated by vacuum filtration using five polymer loadings from a fixed 0.5 mg mL^{-1} aqueous dispersion and were characterized by XRD, ATR-FTIR, and SEM. Their separation performance was evaluated in a dead-end filtration cell at 1 bar using a 10 mg L^{-1} Congo Red feed. Cross-sectional SEM provided the clearest morphological evidence of membrane modification, revealing a distinct granular outer region on the modified membranes that was absent from the bare UF support. In contrast, the ATR-FTIR spectra of the modified membranes remained largely dominated by the UF substrate features and therefore did not independently provide clear evidence of Bipy-PAN deposition. Membrane performance was strongly influenced by polymer loading. Congo Red rejection increased markedly as the Bipy-PAN loading increased from 2.5 to 10 mg, while further increasing the loading produced only limited improvement in rejection and was accompanied by a continued decrease in permeate flux. Consequently, the 10 mg membrane provided the most favorable balance between rejection and flux among the investigated loadings. When this membrane was subsequently evaluated with Congo Red, Acid Red 1, and Methylene Blue, Congo Red exhibited substantially higher rejection than the other two dyes. The observed rejection trend was consistent with an important contribution

from molecular size to the separation behavior; however, the contribution of electrostatic interactions could not be determined conclusively because membrane surface charge and feed pH were not measured. Overall, the findings demonstrate that vacuum-assisted deposition of Bipy-PAN can introduce an effective selective layer onto a commercial UF support, producing a polymer-modified membrane with nanofiltration-type dye-separation behavior, particularly toward Congo Red. Importantly, the results also show that maximizing polymer loading does not necessarily provide the most favorable membrane performance, as the improvement in rejection must be balanced against the accompanying loss in permeate flux. Within the conditions investigated in this work, a Bipy-PAN loading of 10 mg provided the most favorable balance between dye rejection and permeate transport.

References

[1] Guo S, Yan X, Luo Z, Zhang J, Yuan C. Preparation of positively charged nanofiltration membranes: Manipulation of the positive charge. Desalination. 2024;586:117780. doi:10.1016/j.desal.2024.117780.

[2] Alkayal NS. Investigation into the synthetic strategies of melamine-based porous polymeric materials: A bibliometric analysis. Polymers. 2025;17(7):868. doi:10.3390/polym17070868.

[3] Alkayal NS, Alotaibi MM, Tashkandi NY, Alrayyani MA. Synthesis and characterization of bipyridine-based polyaminal network for CO_2 capture. Polymers. 2022;14(18):3746. doi:10.3390/polym14183746.

[4] Qu H, Xiao X, Han Z, Hu M, Shen S, Yang L, Jia F, Wang T, Ye Z, Sun W, Wang Y, Huang L, Zhu Z, Servati P, Tang J, Chen J. Graphene oxide nanofiltration membrane based on three-dimensional size-controllable metal–organic frameworks for water treatment. ACS Appl Nano Mater. 2022;5(4):5196–5207. doi:10.1021/acsanm.2c00234.

[5] Sun J, Hu C, Liu Z, Liu H, Qu J. Surface charge and hydrophilicity improvement of graphene membranes via modification of pore surface oxygen-containing groups to enhance permeability and selectivity. Carbon. 2019;145:140–148. doi:10.1016/j.carbon.2018.12.098

[6] Zhang Z, Jiao J, Jiang Y, Wang Z, Wang J, Cai D, Shan H, Zhao J, Jiao T. Defect engineering strategy of in-situ grown COF-300 nanofiltration membranes for selective dye separation. J Membr Sci. 2026;742:125166. doi:10.1016/j.memsci.2026.125166.

[7] Ge R, Huo T, Nie MX, Lu J, Hou H, Zhan X. In-situ confined preparation of COF@GO nanofiltration membranes for high-efficiency dye removal. Sep Purif Technol. 2025;355:129637. doi:10.1016/j.seppur.2024.129637.

[8] Kertész S, Cakl J, Jiránková H. Submerged hollow fiber microfiltration as a part of hybrid photocatalytic process for dye wastewater treatment. Desalination. 2014;343:106–112. doi:10.1016/j.desal.2013.11.013